Article

Grid Synchronization of Seven-Phase Wind Electric Generator Using d-q PLL

Kalaivani Chandramohan [1], Sanjeevikumar Padmanaban [2,*], Rajambal Kalyanasundaram [1], Mahajan Sagar Bhaskar [2] and Lucian Mihet-Popa [3]

[1] Department of Electrical and Electronics Engineering, Pondicherry Engineering College, Kalapet, Puducherry, India; kalaivani46@pec.edu (K.C.); rajambalk@pec.edu (R.K.)

[2] Department of Electrical and Electronics Engineering, University of Johannesburg, Auckland Park, South Africa; sagar25.mahajan@gmail.com

[3] Faculty of Engineering, Østfold University College, Kobberslagerstredet 5, 1671 Kråkeroy; Building: S 316, Norway; lucian.mihet@hiof.no

* Correspondence: sanjeevi_12@yahoo.co.in; Tel.: +27-79-219-9845

Abstract: The evolving multiphase induction generators (MPIG) with more than three phases are receiving prominence in high power generation systems. This paper aims at the development of a comprehensive model of the wind turbine driven seven-phase induction generator (7PIG) along with necessary the power electronic converters and controller for grid interface. The dynamic model of the system is developed in Maltlab/Simulink. Synchronous reference frame phase-locked loop (SRFPLL) system is incorporated for grid synchronization. The modeling aspects are detailed and the system response is observed for various wind velocities. The effectiveness of seven phase induction generator is demonstrated with the fault tolerant capability and high output power with reduced phase current when compared to conventional 3-phase wind generation scheme. The response of the PLL is analyzed and the results are presented.

Keywords: multi-phase; synchronous frame; induction generator; PWM inverter; seven phase rectifier; PLL; grid

1. Introduction

Electric power generation by exploring the use of renewable energy source is viable solution for reducing the dependency of fast depleting fossil fuels and to fit into the environmental conditions. Among all existing non-conventional sources wind has latent qualities that can be utilized to meet the heaping energy demand [1]. Self-excited induction generators (SEIGs) are usually deployed for wind energy conversion system in standalone applications with its inherent characteristics as mentioned in [2-3]. Later they also operated in grid connected mode for distributed power generation in hybrid micro grids [4]. However they are suitable for low and medium power applications [3]. MPIG with more than three phases is a potential contender which combines the advantages of MPIG with SEIG technologies yielding an efficient, reliable and fault tolerant machine which finds diverse application. [5-8]. Multiphase systems can be employed for different applications, such as offshore energy harvesting, electrical vehicles, electric ship propulsion and aircrafts. The earlier proposed research works brief the supremacy of multiphase machines to obtain a better reliable performance [9-14].

As a consequence, MPIG research has evoked interest among researchers in the recent past which has culminated in to gradual but steady progress in this field. However, available literature suggests finite modeling approaches implemented for MPIG analysis.

The d-q model of six phase induction generator with dual stator and single rotor is presented [15]. The performance of six phase dual stator induction generator is investigated [16]. Dynamic analysis of six phase induction generator for standalone wind power generation [17], steady state performance analysis of the machine and its experimental validation [18-19] has been carried out.

The grid integration of wind electric generator (WEG) is a critical aspect in the planning of wind power generation system. The variation in production and higher intermittency of wind generation makes it difficult for grid integration. Hence it is necessary to provide appropriate synchronization techniques such that the system maintains constant frequency and voltage to ensure stable and reliable operation of grid [20]. A good synchronization method must detect the frequency and phase angle variations proficiently in order to reduce the harmonics and disturbances for safe operation of the grid. Further simple implementation and cost decides the reliability of synchronization scheme [21]. The power transfer between Distributed generation and grid is enhanced by good synchronization method. Earlier known zero crossing detectors have adverse power quality issues during weak grid. Nowadays PLL is one of the generally used techniques and it controls Distributed power generation system and other applications. Several types of PLL are analyzed in [22-23]. This paper aspires at developing a PLL based grid connected seven phase WEG where PLL enables the frequency and voltage synthesis.

A d-q model of seven phase induction generator (7PIG) with stator windings phase shifted by 51.42^0 is developed. Simulation is carried out to study the performance under varying wind velocities. The voltage build up process is shown. The generator voltage, current and power output is presented under varying load conditions. The reliability of the machine under fault condition is examined with one or two phases open. The results are compared with the three phase generator. The power electronic interface namely the seven phase rectifier, boost converter and three phase NPC inverter are simulated for varying modulation indices and results are explored. The SRF PLL is designed to track phase angle and frequency. The response of PLL is analyzed various grid conditions like unbalanced grid voltages, voltage sag, line to line (LL) fault and line to line ground fault (LLG)and the results are explored.

2. Proposed System Description

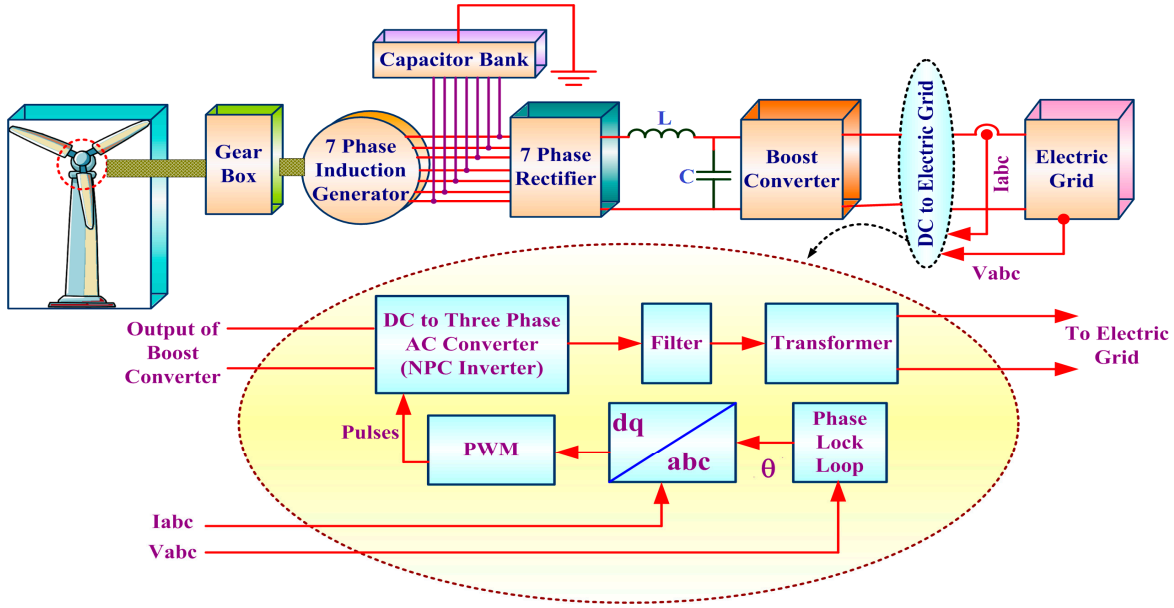

Figure 1. Seven Phase Grid connected Wind electric Generator

The grid connected seven phase wind generation system considered for study consists of Wind turbine drives the 7ϕIG through gearbox. The generated seven phases AC output is rectified by seven phase rectifier and filtered. The filtered and boosted dc output voltage is injected through three phase inverter to grid with proper synchronization through SRF PLL. The inverter is controlled by the synchronous d-q reference frame. Phase lock loop technique incorporated synchronizes the inverter and grid. High frequency ripple at the inverter is filtered. The filtered output of the inverter is fed to grid through step-up transformer.

3. Modeling of System Components

The mathematical modeling of the seven phase wind generator components namely wind turbine, seven phase induction generator, seven phase rectifier and three phase inverter and PLL are discussed in the following sections.

3.1. Wind Turbine

The following equation defines the power output of the wind turbine

$$\rho_{tur} = 0.5\rho A C_p(\lambda) V_w^{\,3} \tag{1}$$

$$C_P = 0.5\left(\frac{116}{\lambda_1} - 0.4\beta - 5\right)e^{\frac{-16.5}{\lambda_1}} \tag{2}$$

$$\lambda = \frac{R\omega_{tur}}{V_w} \tag{3}$$

$$\lambda_1 = \frac{1}{\frac{1}{(\lambda + 0.089)} - \frac{0.035}{(\beta^3 + 1)}} \tag{4}$$

Where,

ρ_{tur} *: Air density (kg/m3);* V_w *- wind velocity (m/s); R - Radius of the wind turbine rotor (m) ; A - Area swept out by the turbine blades (m2) ; Cp: power coefficient defined by equation (2);* λ *- Tip speed ratio given by equation (3)* ω_{tur} *: angular rotor speed of the turbine(rad/sec);* β *: The blade pitch angle (deg.)*

3.2. 7PIG Model

A 7ϕIG has seven stator windings sinusoidally distributed with phase displacement of 51.4º ($360^0/7$) and the rotor is short circuited for squirrel cage induction machine. The7ϕ induction machine operating as generator is represented as a two phase equivalent circuit. The ds-qs represent stator direct and quadrature axes and dr-qr represents rotor direct and quadrature axes. The transformation of seven phase stationary reference frame variables to two phase stationary reference frame is given by equation (5). Assumptions made in modeling 7ϕIG are same as given in [7] and [26]. The modeling 7ϕIG is carried out using d-q equivalent circuit shown if Figure 2 [24-26].

$$\begin{bmatrix} V_q^s \\ V_d^s \\ V_x^s \\ V_y^s \\ . \\ V_o^s \end{bmatrix} = \begin{bmatrix} 1 & \cos\alpha & \cos 2\alpha & \cos 3\alpha & . & \cos n\alpha \\ 0 & \sin\alpha & \sin 2\alpha & \sin 3\alpha & . & \sin n\alpha \\ 1 & \cos 2\alpha & \cos 4\alpha & \cos 6\alpha & . & \cos 2n\alpha \\ 0 & \sin 2\alpha & \sin 4\alpha & \sin 6\alpha & . & \sin 2n\alpha . \\ . & . & . & . & . & . \\ \frac{1}{\sqrt{2}} & \frac{1}{\sqrt{2}} & \frac{1}{\sqrt{2}} & \frac{1}{\sqrt{2}} & . & \frac{1}{\sqrt{2}} \end{bmatrix} X \begin{bmatrix} V_a \\ V_b \\ V_c \\ V_d \\ . \\ V_n \end{bmatrix} \tag{5}$$

Where α=2π/n; n=no of phases; s, r represent stator and rotor quantities; d-q represents direct and quadrature axis.

Equations (5) and (6) defines the stator side voltages

$$V_{qs} = -R_s i_{qs} + \omega\lambda_{ds} + p\lambda_{qs} \tag{6}$$

$$V_{ds} = -R_s i_{ds} - \omega\lambda_{qs} + p\lambda_{ds} \tag{7}$$

Equations (7) and (8) defines the rotor side voltages

Preprints (www.preprints.org) | NOT PEER-REVIEWED | Posted: 11 May 2017 doi:10.20944/preprints201705.0097.v1

Peer-reviewed version available at Energies 2017, 10, 926; doi:10.3390/en10070926

$$V_{qr} = R_r i_{qr} + (\omega - \omega_r)\lambda_{dr} + p\lambda_{qr} \quad (8)$$

$$V_{dr} = R_r i_{dr} - (\omega - \omega_r)\lambda_{qr} + p\lambda_{dr} \quad (9)$$

The voltage equations for dynamic performance analysis under balanced condition are represented in stationary reference frame (ω =0). The rotor side voltages V_{qr} and V_{dr} are zero for squirrel cage induction generators. The rotor side quantities are referred to stator. The flux linkage expression as function of current is given by equations (10) – (15).

$$\lambda_{qs} = -L_{ls} i_{qs} + L_m (i_{qr} - i_{qs}) \quad (10)$$

$$\lambda_{ds} = -L_{ls} i_{ds} + L_m (i_{dr} - i_{ds}) \quad (11)$$

$$\lambda_{qr} = L_{lr} i_{qr} + L_m (i_{qr} - i_{qs}) \quad (12)$$

$$\lambda_{dr} = L_{lr} i_{dr} + L_m (i_{dr} - i_{ds}) \quad (13)$$

$$\lambda_{dm} = L_m (i_{ds} + i_{dr}) \quad (14)$$

$$\lambda_{qm} = L_m (i_{qs} + i_{qr}) \quad (15)$$

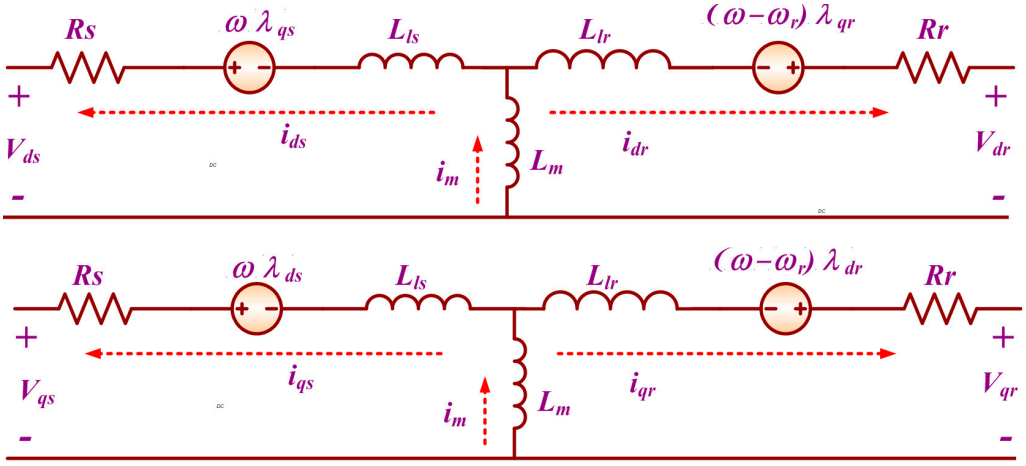

Figure 2. d-q-axis equivalent circuit of 7ϕIG

The leakage inductance of stator and rotor are assumed constant. The degree of magnetic saturation decides magnetizing inductance L_m and it is a non-linear function of magnetizing current which is given by the following equation

$$I_m = \sqrt{(i_{qr} + i_{qs})^2 + (i_{dr} + i_{ds})^2} \quad (16)$$

The non-linear piecewise relationship between the magnetizing inductance and current (L_m,i_m) is given by

$$L_m = \begin{cases} 0.012726, 0 \le i_m < 25.944 \\ 1.94597/(i_m + 117.6), 25.944 \le i_m < 51.512 \\ 1.79031/(i_m + 61.2), 52.512 \le i_m < 73.8 \\ 1.41566/(i_m + 46.296), 73.8 \le i_m < 85.872 \\ 2.67838/(i_m + 31.608), i_m \ge 85.872 \end{cases} \quad (17)$$

The developed electromagnetic torque of the 7ϕIG is defined by

$$T_g = -\frac{7}{2}\left(\frac{P}{2}\right) L_m (i_{qs} i_{dr} - i_{ds} i_{qr}) \quad (18)$$

Negative (-ve) Sign indicates generation action.

$$L_r = L_{lr} + L_m \quad (19)$$

$$L_s = L_{ls} + L_m \tag{20}$$

3.3. Modeling of shunt capacitor and load

The modeling equations of voltage and current of the excitation capacitor and load in d-q axis is given by equations (21) - (26)

$$\rho V_{qs} = \left(\frac{1}{C}\right) i_{cqs} - \omega V_{ds} \tag{21}$$

$$\rho V_{ds} = \left(\frac{1}{C}\right) i_{cds} + \omega V_{qs} \tag{22}$$

$$i_{cqs} = i_{qs} - i_{Rqs} \tag{23}$$

$$i_{cds} = i_{ds} - i_{Rds} \tag{24}$$

$$i_{Rqs} = \frac{V_{qs}}{R} \tag{25}$$

$$i_{Rds} = \frac{V_{ds}}{R} \tag{26}$$

The 7ϕ voltages are transformed to 2ϕ using equation (27).

$$\left.\begin{aligned} V_a &= V_{qs}\cos\theta_e + V_{ds}\sin\theta_e \\ V_b &= V_{qs}\cos(\theta_e - \alpha) + V_{ds}\sin(\theta_e - \alpha) \\ V_c &= V_{qs}\cos(\theta_e - 2\alpha) + V_{ds}\sin(\theta_e - 2\alpha) \\ V_d &= V_{qs}\cos(\theta_e - 3\alpha) + V_{ds}\sin(\theta_e - 3\alpha) \\ V_e &= V_{qs}\cos(\theta_e - 4\alpha) + V_{ds}\sin(\theta_e - 4\alpha) \\ V_f &= V_{qs}\cos(\theta_e - 5\alpha) + V_{ds}\sin(\theta_e - 5\alpha) \\ V_g &= V_{qs}\cos(\theta_e - 6\alpha) + V_{ds}\sin(\theta_e - 6\alpha) \end{aligned}\right\} \tag{27}$$

4. Dc Link Converter

The power electronics based interface system namely the DC link converter involves a seven phase rectifier, three phase inverter and a dc-dc boost converter. The uncontrolled seven phase rectifier converts the seven phase ac output of the generator to dc and is boosted by boost converter.

4.1. Seven phase Diode bridge rectifier

A variable magnitude, variable frequency voltage at the seven phase induction generator terminal is converted to DC using a seven-phase diode bridge rectifier [30].The voltage V_{rec} at the output is given by equation (28) in terms of the peak phase voltage V_{ds} of the generator. The LC filter reduces output voltage ripple of the seven phase rectifier.

$$V_{rec} = \frac{1}{(2\pi/14)} \int_{3\pi/14}^{\pi/2} 1.949 V_{ds} \sin(\omega t + \pi/14) d(\omega t) \tag{28}$$

$$V_{rec} = 1.932 V_{ds} \tag{29}$$

4.2. DC-DC Boost Converter

A DC-DC boost converter steps up the input voltage depending upon duty ratio, inductor and capacitor values [25]. The output voltage of the boost converter is given by

$$V_{dc} = \frac{V_{rec}}{1-\delta} \tag{30}$$

Preprints (www.preprints.org) | NOT PEER-REVIEWED | Posted: 11 May 2017 doi:10.20944/preprints201705.0097.v1

Peer-reviewed version available at Energies 2017, 10, 926; doi:10.3390/en10070926

Where,

V_{rec} - Input voltage from the seven phase rectifier and δ-Duty cycle of the switch. The inductance and capacitance are designed using the following equations (31) and (32).

$$\text{Inductance, } L = \frac{R * \delta(1-\delta)^2}{2 * f_S} \quad \text{(Henry)} \tag{31}$$

$$\text{Capacitance, } C \geq \frac{V_O * \delta}{f_S * \Delta V_O * R} \quad \text{(Farad)} \tag{32}$$

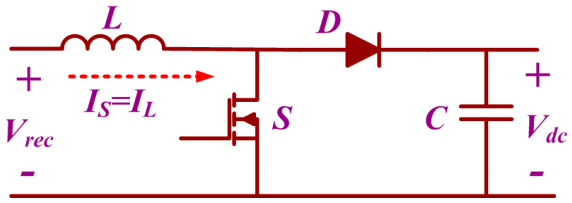

Figure 3. Power Circuit of Boost Converter.

4.3. Three Level Neutral Point Clamped Inverter

The DC input is given to this inverter from the DC/DC converter and three phase three level output obtained is given to the grid through a step-up transformer. The modulation index of the reference signal is varied to control the output voltage of the inverter and is given by relation by

$$\text{Modulation Index, } m_a = \frac{V_m}{V_{dc}/2} \tag{33}$$

Where,

V_m - Peak value of the Phase voltage (V)

V_{dc} - Input DC voltage / Output of the Boost converter

5. Grid Interface using PLL

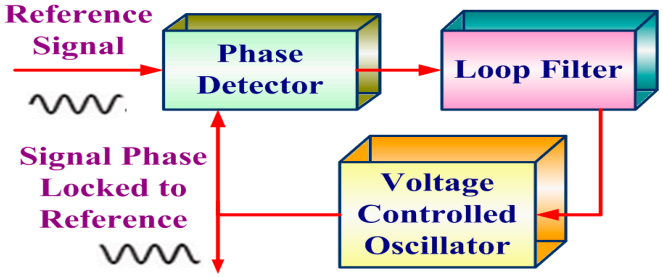

Figure 4. Basic Phase Locked Loop (PLL) Structure.

The effective power transfer between grid and the source can be realized by the efficient synchronization technique. The most familiar method is tracking of phase angle using PLL which synchronizes voltage and frequency of given reference and output signal .A phase detector, loop filter and voltage controlled oscillator (VCO) together makes a basic PLL system wherein phase detector generates an error signal by comparing the reference and output signal. The harmonics of error signal is eliminated by loop filter. Depending on output of loop filter VCO generates the output signal. The basic structure of PLL circuit is as shown in Figure 4. Linear PLL is usually used in single phase system whereas a three phase system employs a SRF PLL or otherwise d-q PLL.

5.1. Synchronous Reference Frame (SRF/d-q) PLL

In the synchronous frame PLL, Clarke's transformation [24] is applied to three-phase voltage vector to transform abc to αβ stationary reference frame. Park's transformation makes αβ to d-q rotating frame as given in Figure 5. The feedback loop controls the angular position of d-q

Preprints (www.preprints.org) | NOT PEER-REVIEWED | Posted: 11 May 2017 doi:10.20944/preprints201705.0097.v1

Peer-reviewed version available at Energies 2017, 10, 926; doi:10.3390/en10070926

reference making the q-axis component zero in steady state. The d-axis will be the voltage amplitude during steady state condition.

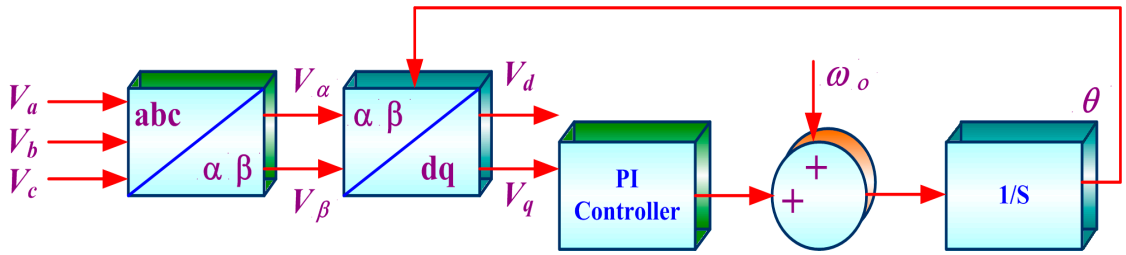

Figure 5. SRF/d-q PLL structure

The d- and q-axis component is defined by the following equation under balanced condition

$$\begin{bmatrix} V_d \\ V_q \end{bmatrix} = \begin{bmatrix} \cos\hat{\theta} & \sin\hat{\theta} \\ -\sin\hat{\theta} & \cos\hat{\theta} \end{bmatrix} \begin{bmatrix} U\cos\theta \\ U\sin\theta \end{bmatrix} = \begin{bmatrix} U\cos(\theta-\hat{\theta}) \\ U\sin(\theta-\hat{\theta}) \end{bmatrix} \quad (34)$$

Where

U, θ – *amplitude and phase of input signal*

$\hat{\theta}$ - *PLL output*

V_d, V_q *are the d and q-axis component*

The phase is denoted by q-axis and amplitude in steady state denoted by d-axis error. The generalized voltage vector under unbalance utility conditions (without voltage harmonics) is represented by

$$V = V_+ + V_- + V_0 \quad (35)$$

The positive, negative and zero sequence components are represented by subscripts +, - and 0. The αβ component using Clarke's transformation is given by

$$V_{\alpha\beta\gamma} = \begin{bmatrix} V_\alpha \\ V_\beta \\ V_\gamma \end{bmatrix} = T_{\alpha\beta/abc} \begin{bmatrix} V_a \\ V_b \\ V_c \end{bmatrix} \quad (36)$$

$$T_{\alpha\beta/abc} = \frac{2}{3} \begin{bmatrix} 1 & \frac{-1}{2} & \frac{-1}{2} \\ 0 & \frac{\sqrt{3}}{2} & \frac{\sqrt{3}}{2} \\ \frac{1}{2} & \frac{1}{2} & \frac{1}{2} \end{bmatrix} \quad (37)$$

The zero-sequence component is neglected as it is on the γ-axis. The expression of the voltage vector on the αβ-plane is:

$$V_{\alpha\beta} = T_{\alpha\beta/abc}(V_+ + V_-) = \begin{bmatrix} U_+\cos\theta_+ + U_-\cos\theta_- \\ U_+\sin\theta_+ + U_-\sin\theta_- \end{bmatrix} \quad (38)$$

The αβ frame is transformed to d-q frame using parks transformation.

$$V_{dq} = T_{dq/\alpha\beta}\ V_{\alpha\beta} = \begin{bmatrix} U_+\cos(\theta_+ - \hat{\theta}) + U_-\cos(\theta_- - \hat{\theta}) \\ U_+\sin(\theta_+ - \hat{\theta}) + U_-\sin(\theta_- - \hat{\theta}) \end{bmatrix} = \begin{bmatrix} U_+ + U_-\cos(2\omega t) \\ U_+ - U_-\sin(2\omega t) \end{bmatrix} \quad (39)$$

$$T_{dq/\alpha\beta} = \begin{bmatrix} \cos\hat{\theta} & \sin\hat{\theta} \\ -\sin\hat{\theta} & \cos\hat{\theta} \end{bmatrix} \quad (40)$$

Peer-reviewed version available at Energies 2017, 10, 926; doi:10.3390/en10070926

ω is the angular frequency of voltage vector and $\hat{\theta} = \theta_+ = \theta_- = \omega t$

6. Simulation Result

The modeling equations of the various system components are simulated with the parameters given in APPENDIX-I. The individual component models are analyzed and integrated to study the performance of the seven phase wind electric generator. The simulation results are discussed in the following sections.

6.1. Wind Turbine

A 250kW wind turbine is simulated using the equations (1) – (4) for various wind velocities and rotational speeds. Figure 6 shows the power curves of the wind turbine at various wind speeds. The rated power of 250kW is achieved at rated wind velocity of 15m/s and 40 rpm as shown in figure 6. The wind turbine produces maximum power at various rotational speeds for different wind velocities.

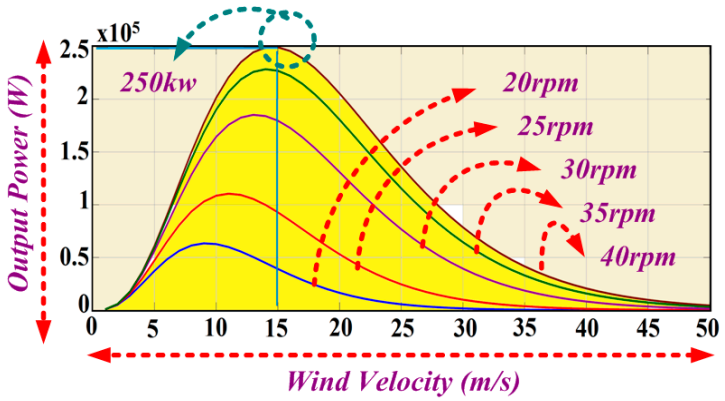

Figure 6. Wind Turbine Power Output Vs Wind Velocity

6.2. Seven Phase Induction Generator

The mathematical equations represented by the equations (5)-(27) is used to develop a mathematical model of 7ϕ induction generator from the d-q equivalent circuit shown in Fig.2. The performance of 7ϕIGis investigated under various operating conditions.

The rated speed of 1018 rpm with the excitation capacitance of 2332 μF is given as input to the generator and the voltage and current of the 7ϕIG are obtained at no load and presented in Figure 7. The self-excitation process begins at time t=0, the stator voltage builds and the steady state value of 419V (peak) and current of about 165Ais reached at t=2.2secs with the phases mutually displaced by 51.4^0 ($2\pi/n$).

The 7PIG is loaded at t=3sec with excitation capacitance held constant at 2332 μF. At t=3sec, the terminal voltage of stator is reduced from 419 volts to 386volts and the current increases from 165A to 241A. The steady state is reached at t=2 secs as shown in figure 8 (a) and figure 8(b). The generated torque and speed of the generator are represented in figure 8 (c) and figure 8(d) which shows for increasing the load, the speed of the generator decreases with increase in torque. The line voltages of seven phase induction generator varies for adjacent (V_{ab}=0.8676Vm) and non-adjacent side (V_{ac}=1.5629V_m) and (V_{ad}=1.949V_m) which is clearly illustrated using the results shown in the figure 9.

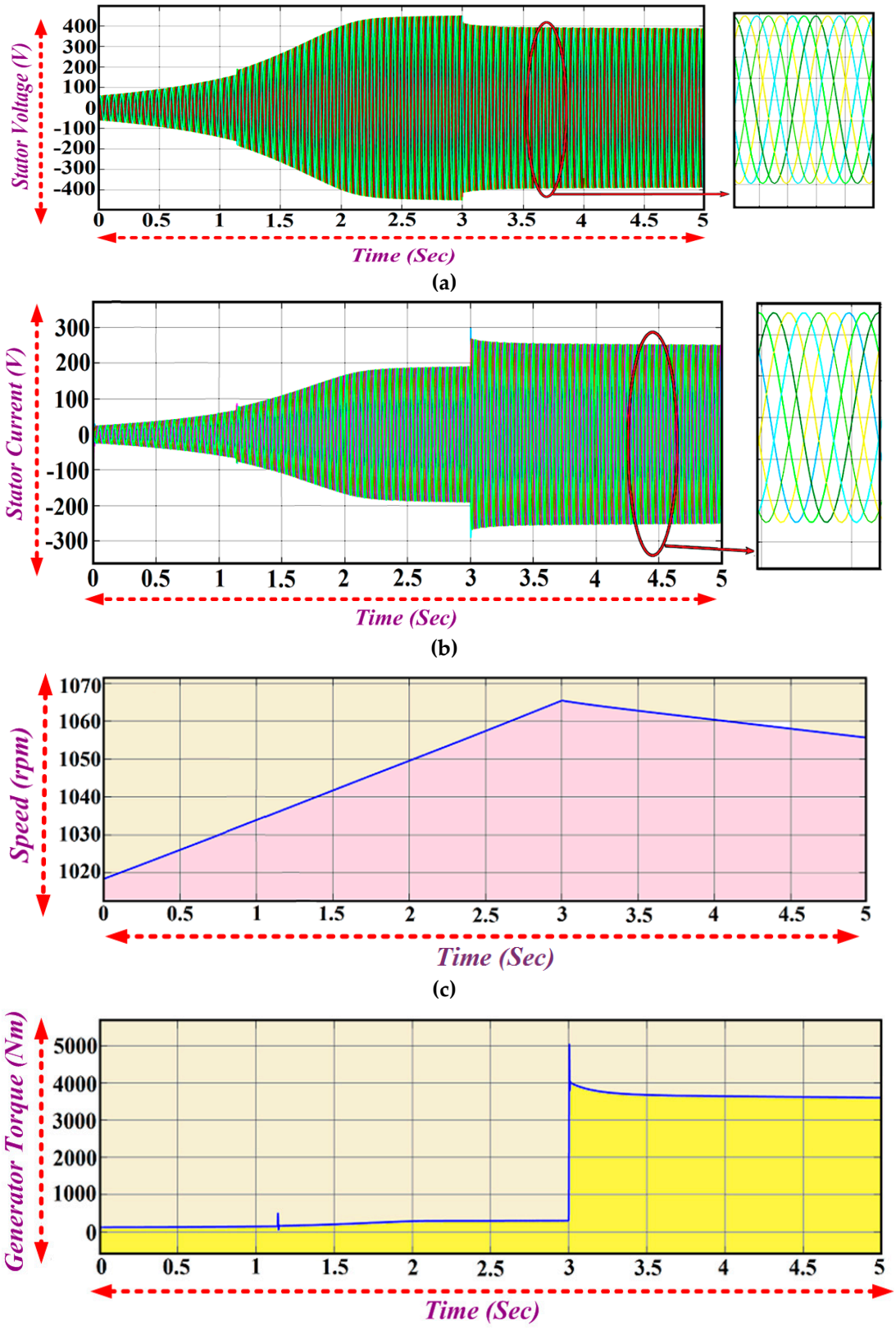

Figure 7. 7ϕIG(a) Output Voltage (b) Current (c) Generator speed (d) Generator Torque

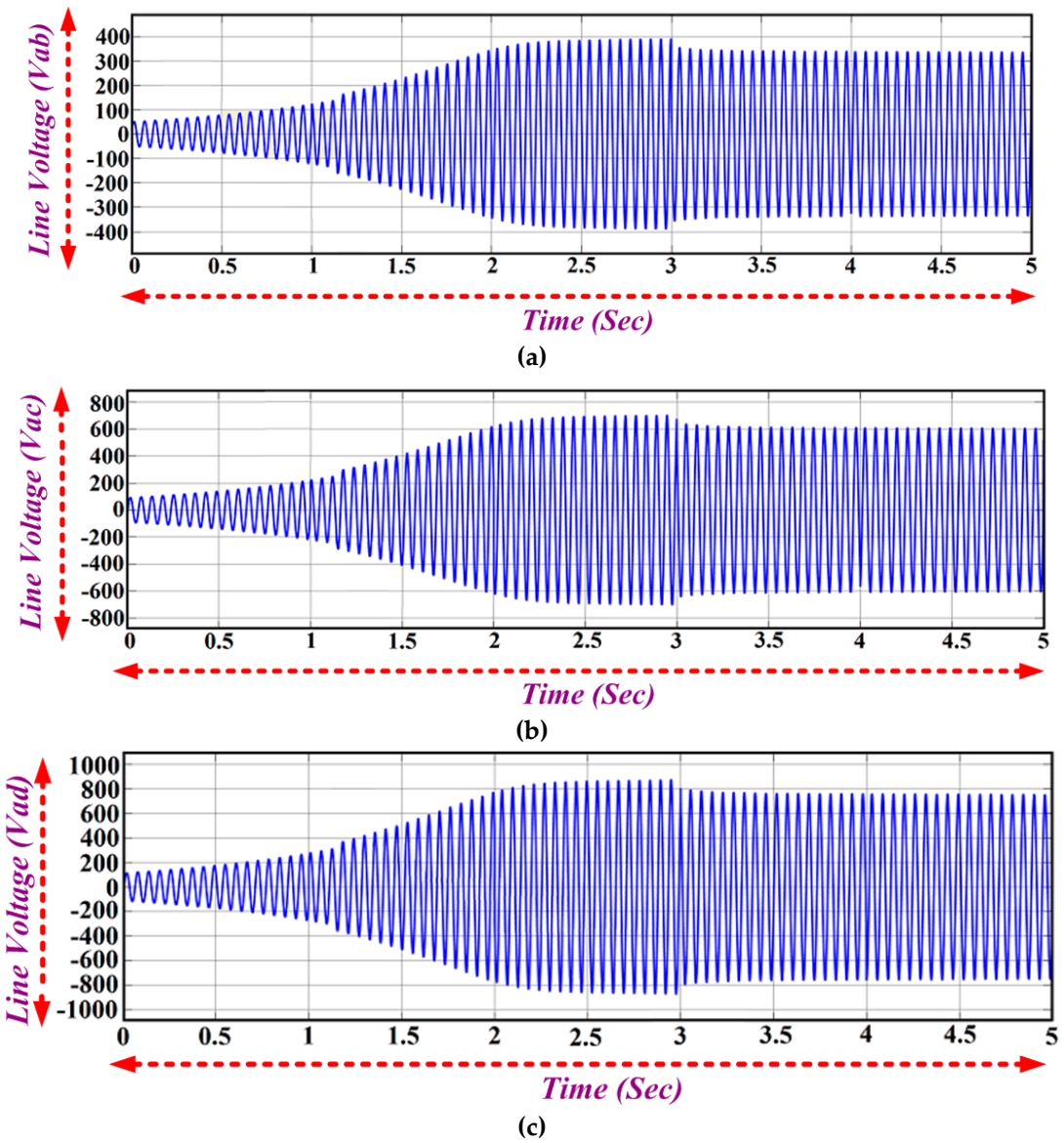

Figure 8. Generated Line Voltage of 7ϕIG Adjacent Side & Non Adjacent Side **(a)** Vab **(b)**Vac **(c)**Vad

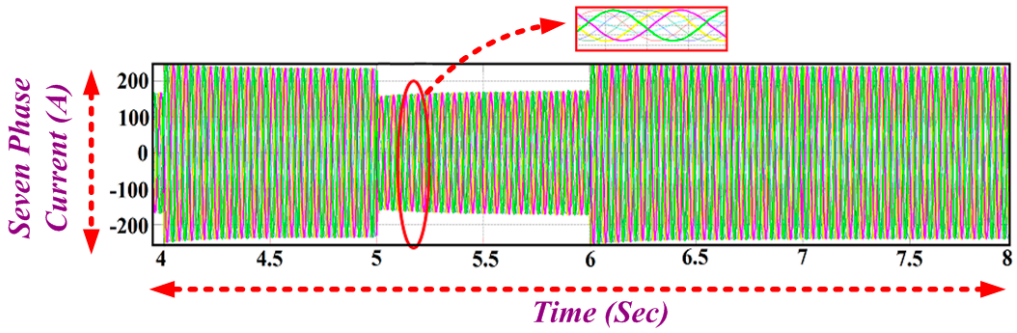

Figure 9. This fault current of 7ϕIG with one phase open (Vc).

6.3. Fault tolerant operation of MPIG

The most important ability of multiphase phase generator is it continues to operate even after the fault in one (or more) phase(s), whereas three-phase machines can hardly realize it. Under the faulty conditions, the additional degrees of freedom available in MPIG are efficiently used for post fault operating strategy. The seven phase generator is operated with one and two phases open circuited V_c, V_c & V_d at t=3secs it is clear from the figure 10 and figure 11 that generator continues to operate with reduced phase current.

Preprints (www.preprints.org) | NOT PEER-REVIEWED | Posted: 11 May 2017 doi:10.20944/preprints201705.0097.v1

Peer-reviewed version available at Energies 2017, 10, 926; doi:10.3390/en10070926

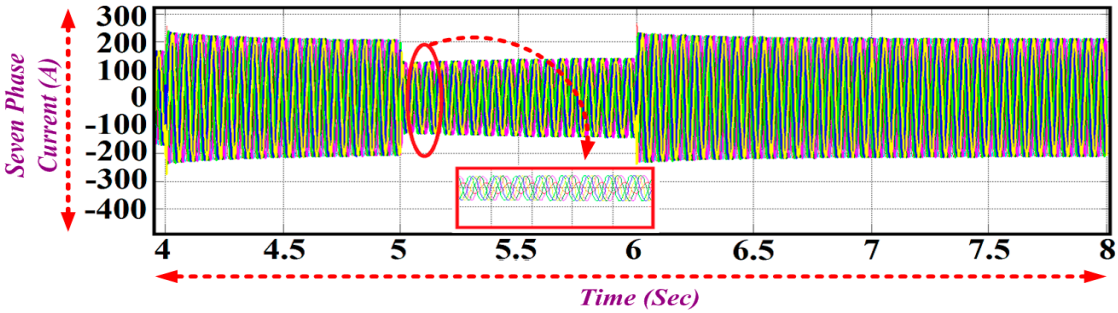

Figure 10. This fault current of 7ϕIG with one phase open (Vc).

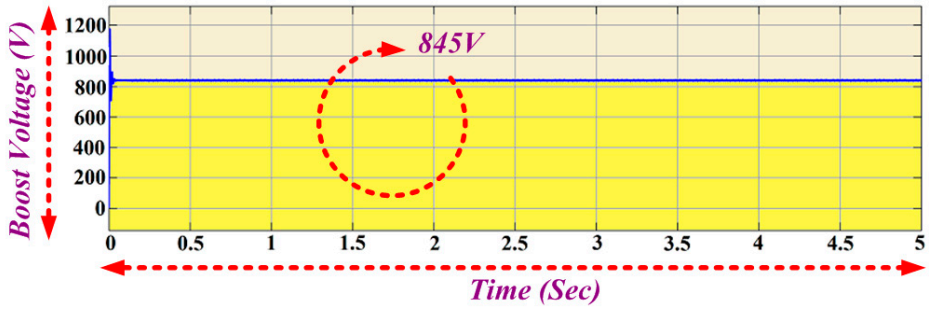

(a)

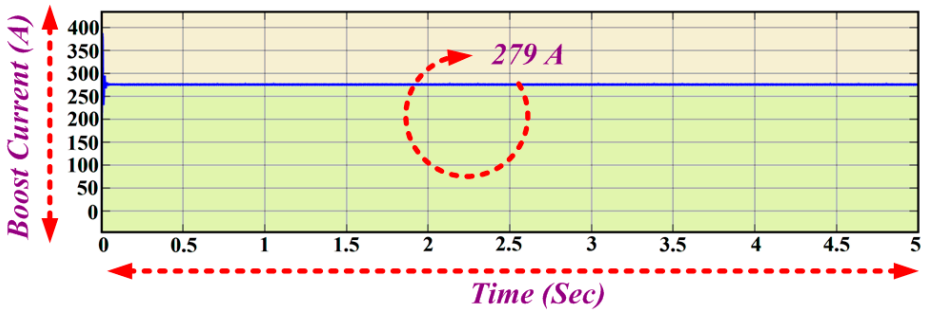

(b)

Figure 11. (a) boost voltage **(b)** Boost current

6.4. DC Link Converter

The generated seven phase ac output is fed input to the seven phase rectifier. The rectified dc output is shown in figure 12. The peak value of phase voltage 386 is fed to rectifier which gives converter 645 volts and a current of 376 A the output of rectifier is fed as input to the converter. The output voltage is found to be 845 V and current of about 279A as shown in figure 10 (a) and (b).

6.5. Grid Integration

The grid tied inverter is the power electronic converter that converts the DC into AC but with the synchronizing qualifications. It is basically used in the applications of the integration of renewable energy to the utility line. The magnitude and phase of the inverter voltage should be as same as that of the grid and its output frequency should be equal to the grid frequency for grid synchronization.

The output of 7P rectifier is given as input to the boost converter. It is clear from figure 11 (a) that 845 volts is obtained and figure 11 (b) shows the modulation index of the inverter. The output phase voltage of the inverter is 365 (peak) and current of about 508 (peak) is achieved as shown in figure 12 .

Preprints (www.preprints.org) | NOT PEER-REVIEWED | Posted: 11 May 2017 doi:10.20944/preprints201705.0097.v1

Peer-reviewed version available at Energies 2017, 10, 926; doi:10.3390/en10070926

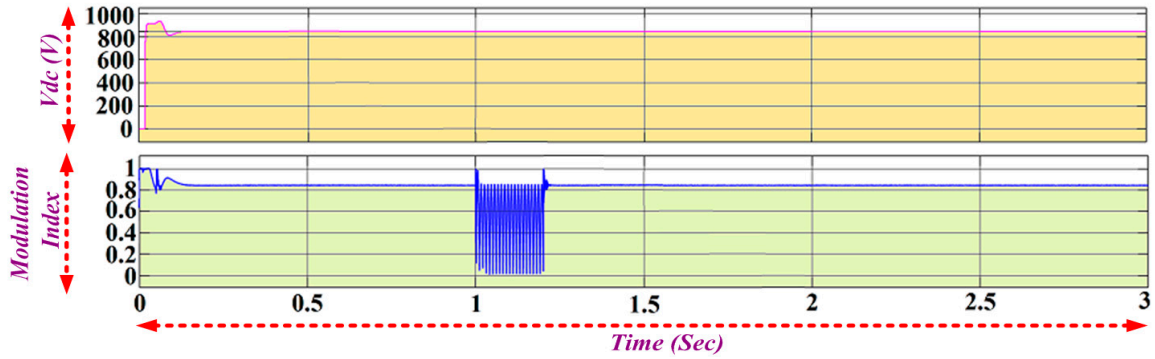

Figure 12. V_{dc} and modulation index

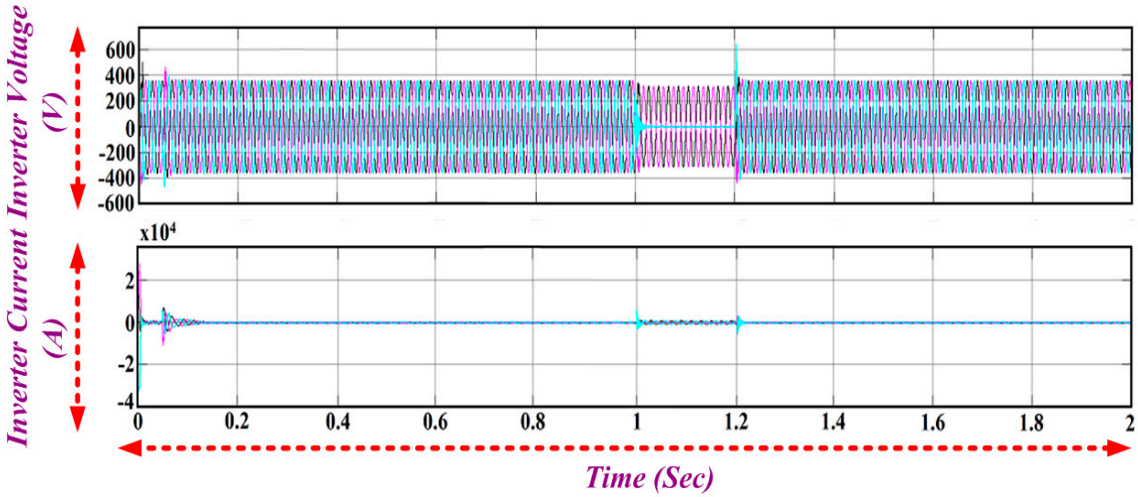

Figure 13. Inverter output voltage and inverter current

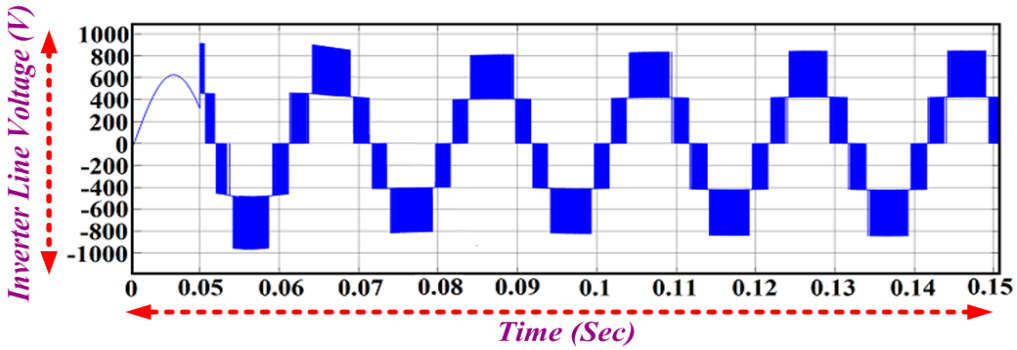

Figure 14. Inverter line voltage

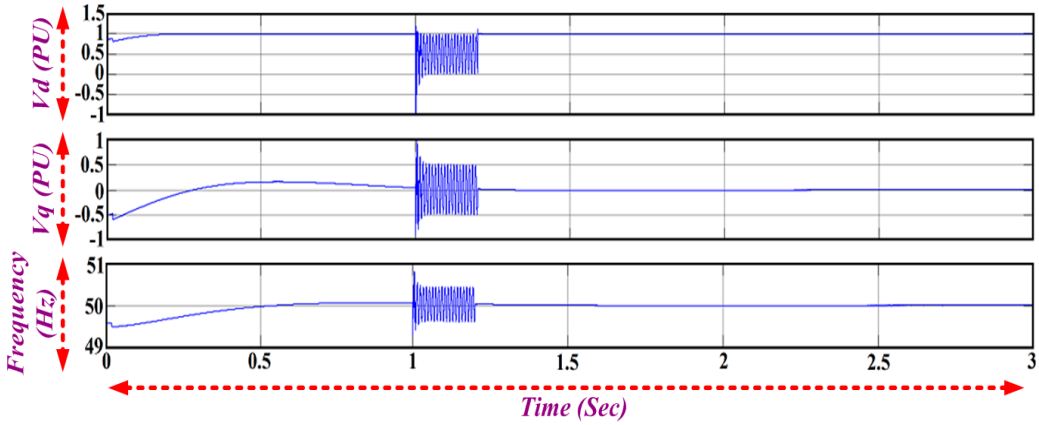

Figure 15. Graph of V_d, V_q and frequency

The d and q axis voltage of d-q PLL and frequency tracking is shown in figure 14. The voltage and current drawn by load connected at point of common coupling is shown in figure 15 (a) and (b). The grid voltage and current is given by figure 16. The power injected into the grid is about 196 kW which is as shown in figure 17.

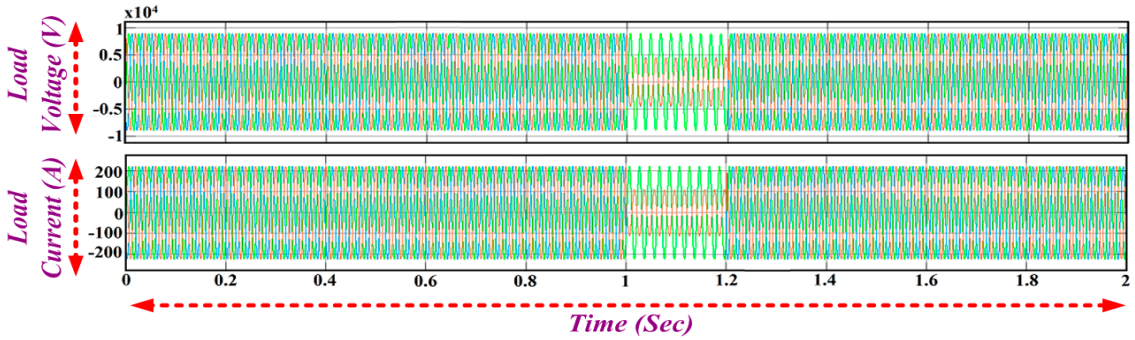

Figure 16. Load Voltage and Load Current

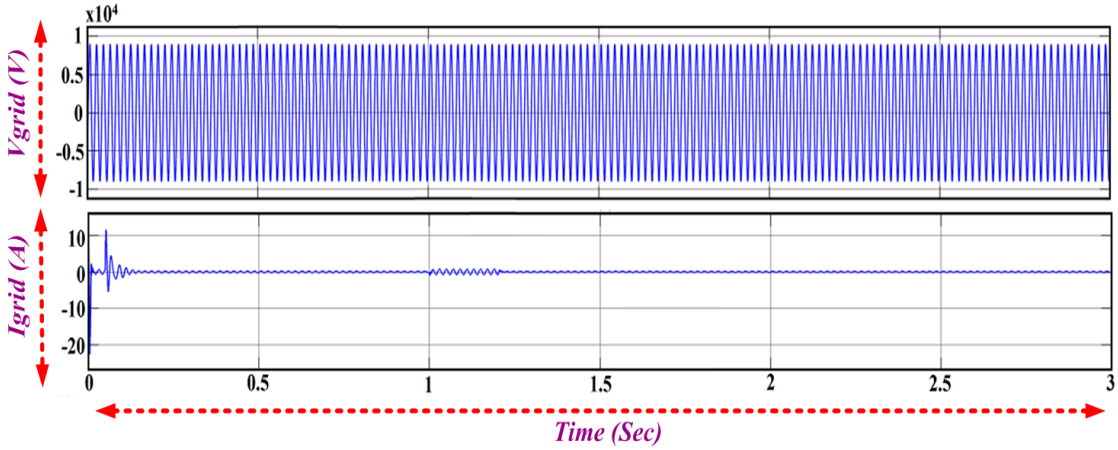

Figure 17. Grid Voltage (Vgrid) and Grid Current (Igrid)

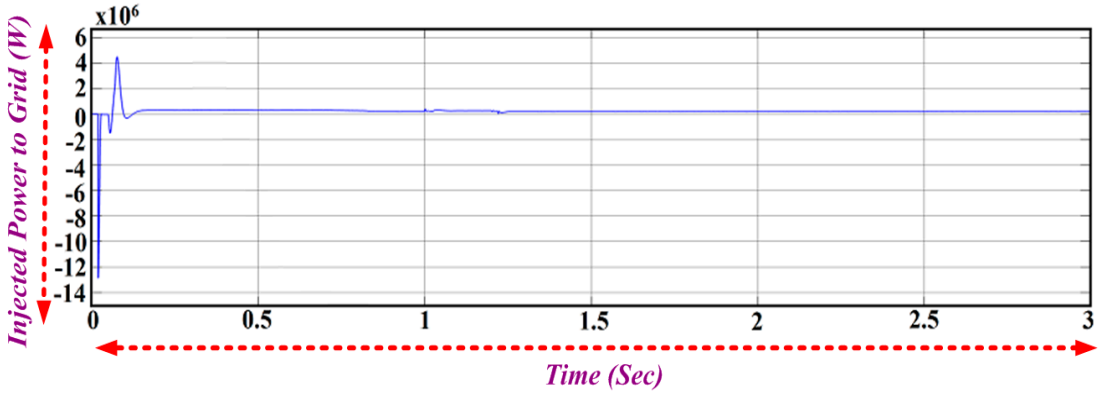

Figure 18. Power injected into the Grid

6.6. SRF PLL performance under various grid Conditions

The grid is subjected to different fault conditions to investigate the performance of SRF PLL. Figure 18 shows the frequency and phase detection variation during line to line fault. It is clear from the fig that phases B and C are in phase with each other and its magnitude is less than phase A whereas the magnitude of phase B and C are zero during line to line ground fault as shown in figure 19(a). The voltages of d-q axis also varies as it contains second harmonic ripples as given by equation (35) which is illustrated by figure 19(b) and figure 19(b).

Preprints (www.preprints.org) | NOT PEER-REVIEWED | Posted: 11 May 2017 doi:10.20944/preprints201705.0097.v1

Peer-reviewed version available at Energies 2017, 10, 926; doi:10.3390/en10070926

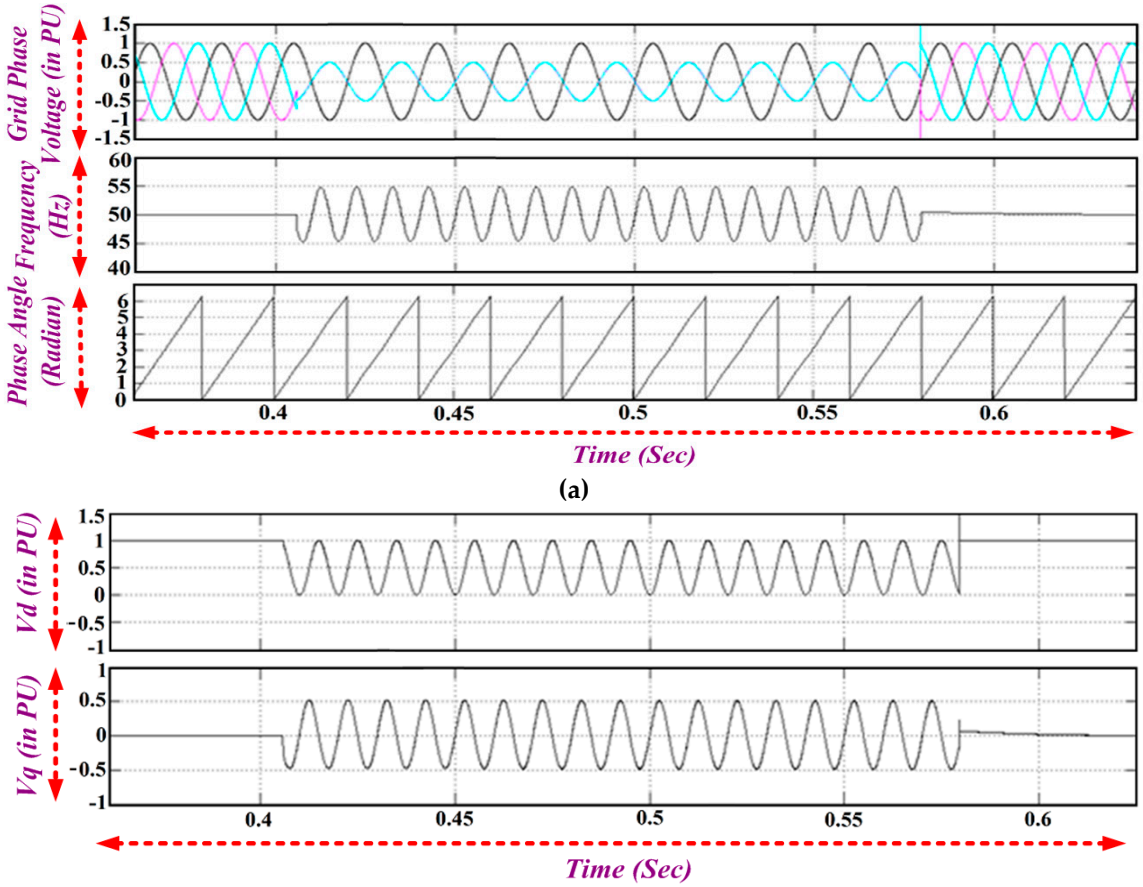

Figure 19. (**a**) Frequency and Phase Angle variation during Line to Line fault (b) q-axis and d- axis voltage magnitude during Line to Line fault

During unbalanced grid voltages, the sinusoidal nature in q axis voltage affects the output of PI controller and generates sinusoidal error signal and hence sinusoidal angular frequency this is shown in figure 20 (a) and figure 20(b) which is similar to line to line fault. SRF PLL performance during voltage sag is shown in figure 21(a) and figure 21(b). Voltage sag condition occurs in grid such that magnitude of all phase voltages are equal and their magnitudes are 50% of nominal voltage. It is noticed that it doesn't cause any oscillations in the frequency and the q-d axis voltages. Balanced voltage sag doesn't affect PLL tracking. However, sudden change in magnitude cause the dip in estimated frequency of SRF PLL and later SRF PLL tracks the phase angle of the grid voltages.

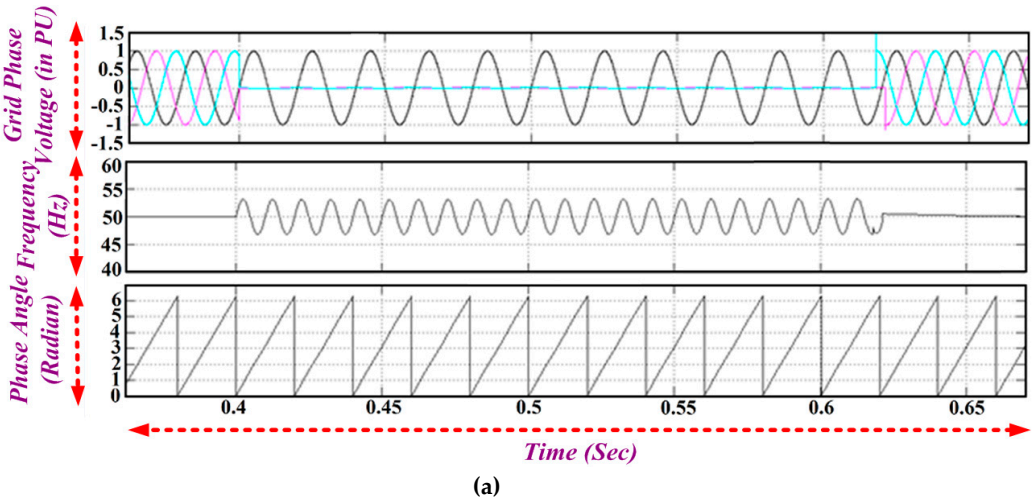

Preprints (www.preprints.org) | NOT PEER-REVIEWED | Posted: 11 May 2017 doi:10.20944/preprints201705.0097.v1

Peer-reviewed version available at Energies 2017, 10, 926; doi:10.3390/en10070926

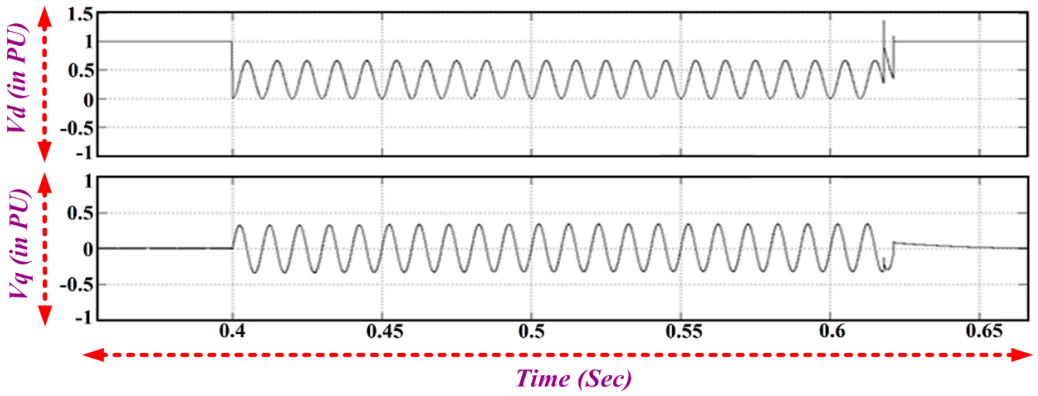

(b)

Figure 20. (**a**) Frequency and Phase Angle variation during LLG fault (**b**) Description of what is contained in the second panel. Figures should be placed in the main text near to the first time they are cited. A caption on a single line should be centered.

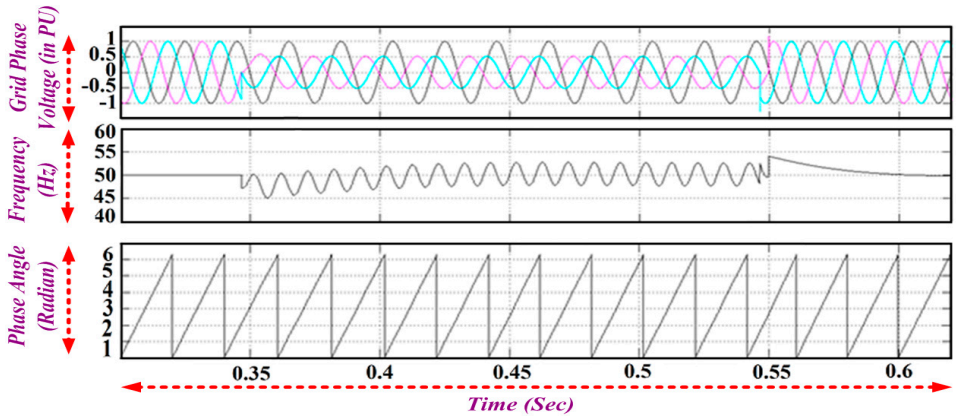

(a)

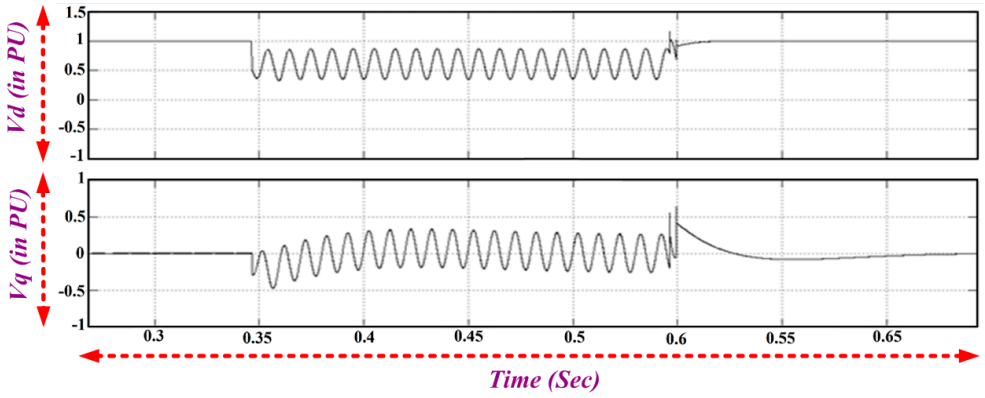

(b)

Figure 21. (**a**) Frequency and Phase detection variation during unbalanced grid voltages (**b**) q-axis and d- axis voltage magnitude during unbalanced grid voltages

Preprints (www.preprints.org) | NOT PEER-REVIEWED | Posted: 11 May 2017 doi:10.20944/preprints201705.0097.v1

Peer-reviewed version available at Energies 2017, 10, 926; doi:10.3390/en10070926

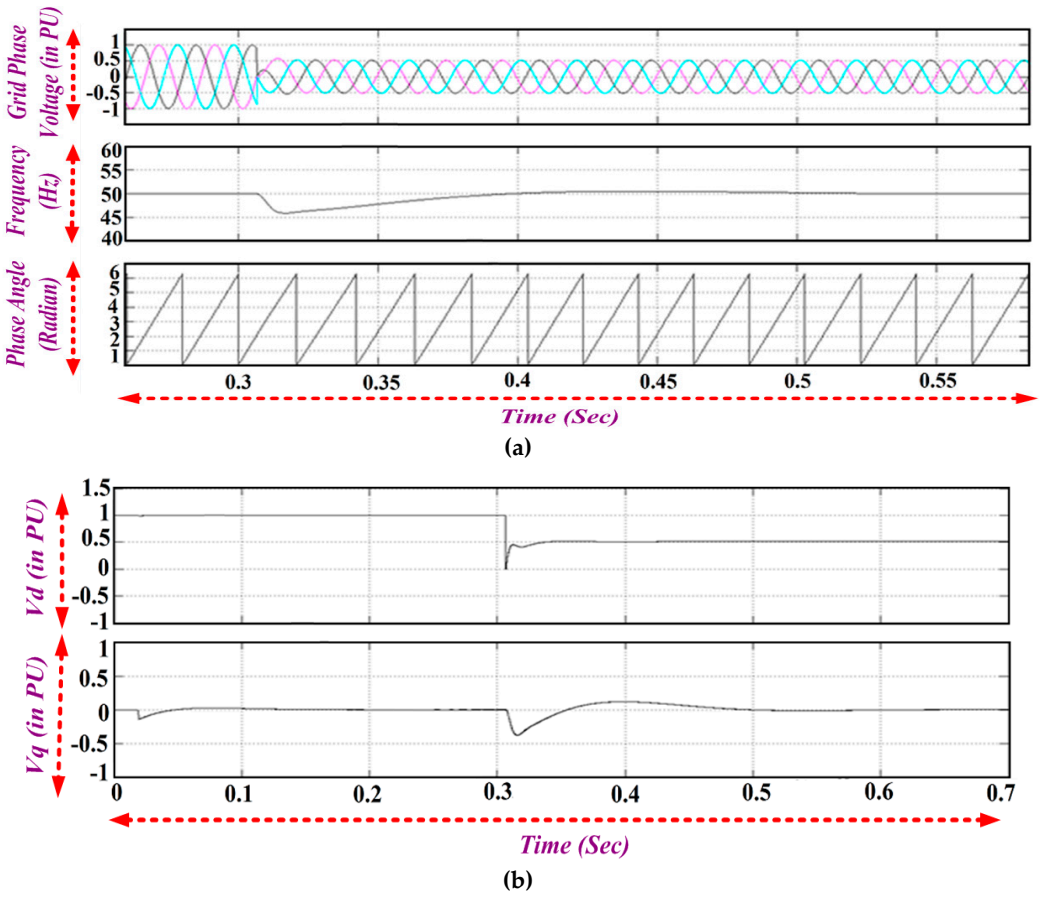

Figure 22. (**a**) Frequency and Phase detection variation during voltage sag (**b**) q-axis and d-axis voltage magnitude during voltage sag.

5. Conclusions

In this article, a comprehensive model of wind driven 7ϕIG in grid connected mode is developed using the two axis d-q equivalent circuit. Seven phase wind electric generator is integrated using the individual system components and the performance of seven phase wind electric generator is analyzed for varying wind velocities. Synchronous reference frame PLL incorporated for grid interface is simulated and analyzed. The enhanced performance 7PIGis evaluated through fault tolerant capability and high output power with reduced current per phase when compared with three phase. The performance SRF-PLL incorporated in grid connected seven phase wind electric generator is analyzed for various operating grid conditions. The use of multiphase machines along with PLL synchronization of grid increases the reliability of the WEG due to the possibility of achieving post-fault disturbance free operation provided by seven phase machine more over constant voltage and frequency operation enabled by d-q PLL.

Appendix A

Wind Turbine		7PIG	
Rated power	250kW	Rated power	210 kW
No. of blades	3	Rated voltage	240V
Rated speed	40rpm	Rated current	240A
Rotor Diameter	29.8m	Rated frequency	50Hz
Air density	1.2kg/m^3	Rated power factor	0.82
Blade pitch angle	-1.1	Rated speed	1018rpm
Gear Ratio	1:24.52	No. of poles	6

Cut-in wind speed	3m/s	Stator resistance	0.12 ohms
Cut-out wind speed	25m/s	Stator leakage inductance	0.017197mH
Rated wind speed	15m/s	Rotor resistance referred to stator	0.0047ohms
Equivalent inertia	1542 kg-m^2	Rotor leakage inductance referred to stator	0.015605mH

References

1. Yaramasu, V,; Bin, Wu; Sen, P, C; and et.al. High-power wind energy con-version system: state-of-the-art and emerging technologies,*IEEE Proc.*, vol.103, no.5, pp.740-788, 2015.
2. G, K, Singh. Self-Excited Inducation Generator Research – a survey, journal on Electric power systems research, Elsevier 69; 107-114,
3. R, C, Bansal. Three phase self-excited induction generator-an overview, IEEE Transactions On Energy Conversion, Vol. 20, No. 2, June 2005.
4. Thomsen, B;' Guerrero, J and Thogersen, P. Faroe islands wind-powered space heating microgrid using self-excited 220-kW induction generator. IEEE Transaction Sustainable Energy, vol. 5, 1361–1366, 2014.
5. Khan, M, F and et al. Modeling, implementation and analysis of a high (six) phase self-excited induction generator. JESIT, http://dx.doi.org/10.1016/j.jesit.2016.12.016 , (2017).
6. Levi. Analysis of double stator induction machine used for a variable speed constant frequency small scale hydro/wind electric generator. Electric Power System Research; vol. 11, 1986.
7. E, Levi; R, Bojoi; F, Profumo; H, A, Toliyat and S, Williamson. Multiphase induction motor drives – a technology status review. IET Electronics Power Application, vol.1, pp. 489–516, 2007.
8. G, K, Singh. Multiphase Induction Machine drive research. Elsevier Journal, Electric Power System Research, Vol. 61, pp. 139-147, 2002.
9. Jones M and Levi E. A literature survey of state-of-the-art in multi-phase ac drives. In Proc. 36th Univ. Power Eng. Conf. UPEC; p p. 505–10, Stafford, 2002,
10. Apsley, J, M,; Williamson, S,; Simth, A, and Barnes, M. Induction machine performance as a function of phase number. IEE Proc. Electron. Power Appl., Vol. 153, No. 6, pp.898-904, 2006
11. Apsley, J and Williamson, S. Analysis of multiphase induction machines with winding faults. IEEE Trans. Ind. Appl., Vol. 42, No. 2, pp. 465-472, 2006.
12. T, Wang; F, Fang; X, Wu; and X, Jiang. Novel Filter for Stator Harmonic Currents Reduction in Six-Step Converter Fed Multiphase Induction Motor Drives. IEEE Transactions On Power Electronics, Vol. 28, No. 1, 2013
13. Ayman S; Abdel-Khalik and Shehab Ahmed. Performance Evaluation of a Five-Phase Modular Winding Induction Machine. IEEE Transactions on Industrial Electronics, vol. 59, no. 6, june 2012.
14. Ayman S; Abdel-Khalik and M, Masoud. Effect of Current Harmonic Injection on Constant Rotor Volume Multiphase Induction Machine Stators: A Comparative Study. IEEE Transactions on Industry Applications, Vol. 48, No. 6, November/December 2012.
15. Singh G, K; Yadav KB and Saini RP. Modeling and analysis of multi-phase (six phase) self-excited induction generator. In: Proc. IEEE Conf. The Eighth International Conference on Electrical Machines And Systems, ICEMS'05, vol. 3; 2005.
16. Singh G, K; Yadav KB and Saini RP. Analysis of a saturated multi-phase (six-phase) self-excited induction generator. International Journal Emerging Electr. Power System Vol.7, 2006.
17. Singh G, K. Modeling and experimental analysis of a self-excited six-phase induction generator for stand-alone renewable energy generation. Internation Journal Renew Energy, Vol.33, 2008.
18. Singh G, K; Yadav K, B and Saini R,P. Capacitive self-excitation in six-phase induction generator for small hydro power – an experimental investigation. In: Proc. IEEE conf. power electronics, drives and energy systems, PEDES-2006

19. Singh G,K. Steady-state performance analysis of six-phase self-excited induction generator for renewable energy generation. In: Proc. the 11th Int. Conf. on Electrical Machines And Systems, ICEMS, 2008
20. Mittal, R; Sandhu, K, S and Jain, D,K. An overview of some important issues related to wind energy conversion system (WECS). Int. J. Environ. Sci. Dev. vol.1 , Oct 2004.
21. F, Blaabjerg; M, Liserre; and K, Ma. Power Electronics Converters for Wind Turbine Systems. IEEE Transactions on Industry Applications, vol.48(2), 2012.
22. L, R, Limongi; R, Bojoi; C, Pica; F, Profumo and A, Tenconi. Analysis and Comparison of Phase Locked Loop Techniques for Grid Utility Applications. Proc. IEEE Power Conversion Conf. PCC, pp. 674-681, 2007.
23. M, Karimi-Ghartemani and M, Iravani. A method for synchronization of power electronic converters in polluted and variable-frequency environments. IEEE Trans. Power System, vol.19, no. 3, pp. 1263–1270, Aug. 2004.
24. P, C, Krause. Analysis of Electric Machinery and Drive systems. Wiley *IEEE Press*, 2013
25. Bimal, K, Bose. Modern Power Electronics and AC Drives. Prentice Hall, USA, 2002
26. Renukadevi, G, and Rajambal, K. Generalized model of multi-phase induction motor drive using Matlab/Simulink. Int. IEEE PES Conf. Innovative Smart Grid Technologies, Kerala, India, 2011
27. Renukadevi, G, and Rajambal, K,; Novel carrier-based PWM technique for n-phase VSI. International Journal Energy Technology, vol.1(3), pp. 1-9, 2011.
28. G, Renukadevi and K,Rajambal. Comparison of different PWM schemes for n –phase VSI. In Proc. International Conference on Advances In Engineering, Science And Management pp.559-564, March 2012.
29. Renukadevi, G,; and K, Rajambal. Field programmable gate array implementation of space-vector pulse-width modulation technique for five-phase voltage source inverter. IET Power Electronics ,Vol.7 (2), pp.376-389, 2014.
30. M, Masoud. Five-phase Uncontrolled Line Commutated Rectifier: AC Side Compensation using Shunt Active Power Filter. Proceedings of the 8th IEEE GCC Conference and Exhibition, Oman, February2015

Acknowledgments: No funding resources.

Author Contributions: Kalaivani Chandramohan, Sanjeevikumar Padmanaban, and Rajambal Kalyanasundaram, has developed the concept of the research proposed and developed the numerical background; Mahajan Sagar Bhaskar involved in the implementation of numerical simulation along with other authors for its depiction in quality of the work with predicted output results. Lucian Mihet-Popa has contributed his experience in AC drives and Wind Energy Conversion for further development and verification of theoretical concepts. All authors involved in articulating the paper work in its current form in each part their contribution to research investigation.

Conflicts of Interest: "The authors declare no conflict of interest."